

# Run-and-tumble particles in speckle fields

M. Paoluzzi, R. Di Leonardo, and L. Angelani

CNR-IPCF, UOS Roma, Dip. Fisica, Università *Sapienza*, P. le A. Moro 2, I-00185, Rome, Italy

E-mail: [matteo.paoluzzi@ipcf.cnr.it](mailto:matteo.paoluzzi@ipcf.cnr.it)

**Abstract.** The random energy landscapes developed by speckle fields can be used to confine and manipulate a large number of micro-particles with a single laser beam. By means of molecular dynamics simulations, we investigate the static and dynamic properties of an active suspension of swimming bacteria embedded into speckle patterns. Looking at the correlation of the density fluctuations and the equilibrium density profiles, we observe a crossover phenomenon when the forces exerted by the speckles are equal to the bacteria's propulsion.

## 1. Introduction

Starting from the seminal paper of Ashkin [1], optical trapping has developed into a powerful technique, widely used in many scientific areas, to manipulate atoms [2], Bose-Einstein condensate [3], viruses and bacteria [4]. By means of holographic optical tweezers it is possible to trap array of particles or molecules in three dimensions [5, 6]. More recently it has been demonstrated that a static speckle pattern, generated by the interference of random coherent wavefronts, can trap and manipulate a large number of particles in three dimensions [7]. Brownian motion in random energy landscapes provides useful models to study theoretically and experimentally different phenomena like anomalous transport in inhomogeneous media [8, 9, 10, 11, 12, 13], the relaxation properties of disordered and glassy materials [15, 14, 16, 9], anomalous diffusion in living matter [17] and in disordered media [18, 19]. Colloids in one [20, 21] and two dimensional [22] random energy landscapes have been recently investigated in experiments and by means of numerical simulations [23]. While many efforts have been devoted to study passive particles in random potentials, the behavior of active objects has been only recently explored [24, 25].

We investigate the dynamics of active particles in the energy landscape provided by speckle patterns. The microscopic dynamics that we will address, namely run-and-tumble [26], mimics the motion of swimming bacteria as *E. coli* [27, 28, 29, 30]. Run-and-tumble is a simple but powerful model that captures many properties of motile bacteria [26, 31, 32, 33]. From the theoretical point of view, in the non-interacting limit (“ideal gas” of active particles with no steric interactions), density fluctuations can be computed analytically in one, two and three dimensions [34, 35]. The exact theory has been used to map interacting bacterial baths into an effective non-interacting system [36]. Run-and-tumble is analytical tractable to study sedimentation and harmonic trapping [37], rectification [37, 38], first-passage time problems in one dimension [39], self-trapping and collective phenomena [40]. By means of run-and-tumble model, ratchet phenomena can be studied analytically [37, 38] and through numerical simulations [41, 42, 43].

A central quantity in run-and-tumble dynamics is the persistence length  $l = v_0/\lambda$  that is fixed by both the tumbling rate  $\lambda$ , and the self-propulsion velocity  $v_0$ . The persistence length sets the crossover between a ballistic regime at short length scales and a diffusive regime over long distances. The diffusive regime is characterised by a diffusivity  $D = v_0^2/d\lambda$  [31] with  $d$  the dimensionality of the space. Generalizing the Stokes-Einstein equation we can associate to run and tumble particles an effective thermal energy scale defined by  $D = \mu k_B T_{eff}$  where  $\mu$  is the mobility. In many situations active particles have been actually found to behave like hot colloids [44] with an effective temperature given by  $T_{eff}$  [37]. However, at variance with Brownian motion, where the thermal noise is practically unbounded, the propelling force in swimming bacteria has a finite value that sets the maximum slope that bacteria can climb when escaping from an energy barrier.

We used numerical simulations to study the dynamics of run and tumble bacteria

moving in the random energy landscape generated by the intensity of a speckle field. When increasing the overall intensity of speckles, we observe a crossover between a homogeneous and an inhomogeneous density regime where the density is enhanced on the intensity maxima of the speckles. The crossover is characterised by a decrease in the configurational entropy and by the emergence of a plateau in the collective part of the intermediate scattering function. A similar crossover is expected to occur for Brownian particles when the average value of the random energy landscape increases above the thermal energy scale  $k_B T$ . Here we found that the crossover for active particles occurs before the average landscape energy reaches  $k_B T_{eff}$ . A much better estimate for the position of the crossover is obtained by equating the maximum external force to the propelling force of bacteria.

The paper is organized as follows. In Sec. 2 we introduce the model for the speckle field, in Sec. 3 we illustrate the numerical methods, in Sec. 4 we present and discuss the results.

## 2. Speckle field in numerical simulations

A speckle field can be obtained as the superposition of  $N_m$  Fourier modes where both wave vectors and phases are randomly chosen:

$$\varphi(\mathbf{r}) = c \sqrt{\frac{k_B T_{eff}}{N_m}} \sum_l e^{i(\mathbf{r} \cdot \mathbf{k}_l + \theta_l)}, \quad (1)$$

with  $\mathbf{r} = (x, y)$ . Imposing periodic boundary conditions  $\mathbf{k}_l = (2\pi/L)(l_x \hat{x} + l_y \hat{y})$ , where  $L$  is the box length and  $l_x, l_y$  are random positive and negative integers satisfying the condition  $|\mathbf{k}_l| < 2\pi/\ell$  with  $\ell$  the cell length. The random phases  $\theta_l$  are uniformly distributed between 0 and  $2\pi$ . The square modulus of  $\varphi(\mathbf{r})$  is a real scalar function having the dimensions of energy and an exponential distribution [45] with average  $c^2 k_B T_{eff}$ . The parameter  $c$  is a dimensionless number that tunes the intensity of the forces. As discussed in the following, we model steric interactions between elongated cell bodies using two force centers arranged along the cell axis. The mechanical action of speckles is consequently calculated as a system of forces acting on the same two centers and equal to the gradient of the speckles intensity:

$$I(\mathbf{r}) = \{\Re[\varphi(\mathbf{r})]\}^2 + \{\Im[\varphi(\mathbf{r})]\}^2, \quad (2)$$

where  $\Re$  and  $\Im$  are respectively the real and the imaginary part. The forces due to the field attract bacteria towards region of high intensity and can be expressed as

$$\mathbf{f}_{ext}(\mathbf{r}) = -\nabla U(\mathbf{r}) \quad (3)$$

where the potential  $U(\mathbf{r})$  is

$$U(\mathbf{r}) = -I(\mathbf{r}). \quad (4)$$

From Eq. (4) follows that speckles play the role of a random energy landscape [10]. The maximum value of the energy is zero, and the energy of the local minima, i. e., the

light spot of the speckles, depends on the local intensity of the light. In the following we will consider two cases. The first one is the usual speckle field obtained from the interference of the random Fourier modes

$$U_1(\mathbf{r}) = -\{\Re[\varphi(\mathbf{r})]\}^2 - \{\Im[\varphi(\mathbf{r})]\}^2 \quad (5)$$

The second case is obtained taking only the real part of  $\varphi$ :

$$U_2(\mathbf{r}) = -2\{\Re[\varphi(\mathbf{r})]\}^2 \quad (6)$$

giving rise to slight different spatial pattern and that can be easily obtained in a laboratory with the aid of spatial light modulators. The real and imaginary parts of  $\varphi(\mathbf{r})$  vanish over independent curved paths on the  $x, y$  plane [45]. This implies that while  $U_1$  only vanishes at the intersection points of those paths,  $U_2$  goes to zero over the entire length of the paths  $\Re[\varphi(\mathbf{r})] = 0$ . Therefore, when the average energy in the two potentials is equal, we expect to observe larger spatial gradients, and hence forces, for  $U_2$ . The speckle patterns used in the simulations are generated using the same realization of  $N_m = 500$  wave numbers and phases. The intensity of the speckles for  $c = 0.165$  are shown in the top of panel (a) of Fig. (1) ( $U_1$  in the left of the panel (a) and  $U_2$  in the right of the same panel). In the bottom of the panel (a) we show the contour plot of the modulus of the force field. The two patterns contain the same energy but, as we can see from the contour plot of the modulus of the forces, the speckle  $U_2$  exerts greater forces than  $U_1$ .

In the panel (b) of Fig. (1) we report the probability distribution of the force for the patterns used in the simulations. In unit of  $f_0$ , the self propulsion of the swimmer, setting  $c = 1.0$ , the mean value is 2.4 for  $U_1$  and 3.0 for  $U_2$ . The maximum force is 13.8 for  $U_1$  and 27.5 for  $U_2$ . Using the parameter  $c$  to control the intensity of the speckle, the mean force acting on entire the swimmer equals the self propulsion when  $c = 0.460$  for  $U_1$  and  $c = 0.410$  for  $U_2$ . Looking at the maximum value of the force, the self propulsion is matched at  $c = 0.190$  for  $U_1$  and  $c = 0.135$  for  $U_2$ .

In the panel (c) of Fig. (1) we show the probability distribution of the maximum value of force for  $U_1(\mathbf{r})$  and  $U_2(\mathbf{r})$ . The figure is obtained averaging over  $N_s = 3000$  samples of speckles with same energy. As expected, according to the shape of the distribution the speckle  $U_2(\mathbf{r})$  is characterized by a long tail for large values of  $f$ .

### 3. Molecular Dynamics Simulations

#### 3.1. Run-and-Tumble dynamics

We perform numerical simulations of run-and-tumble dynamics in two dimensions. Considering a system of  $N$  self-propelled swimmers each of length  $\ell$  and thickness  $a$  (for a detailed discussion of the model see [41, 42, 43]), the swimmer is modeled by a unit vector  $\mathbf{e}_i$ , representing the swimming direction, and two short-range repulsive force-centers (beads) arranged along it. The position of the two beads of the  $i$ -th cell is labelled by greek symbols (the swimmers are represented in Fig. (2)).

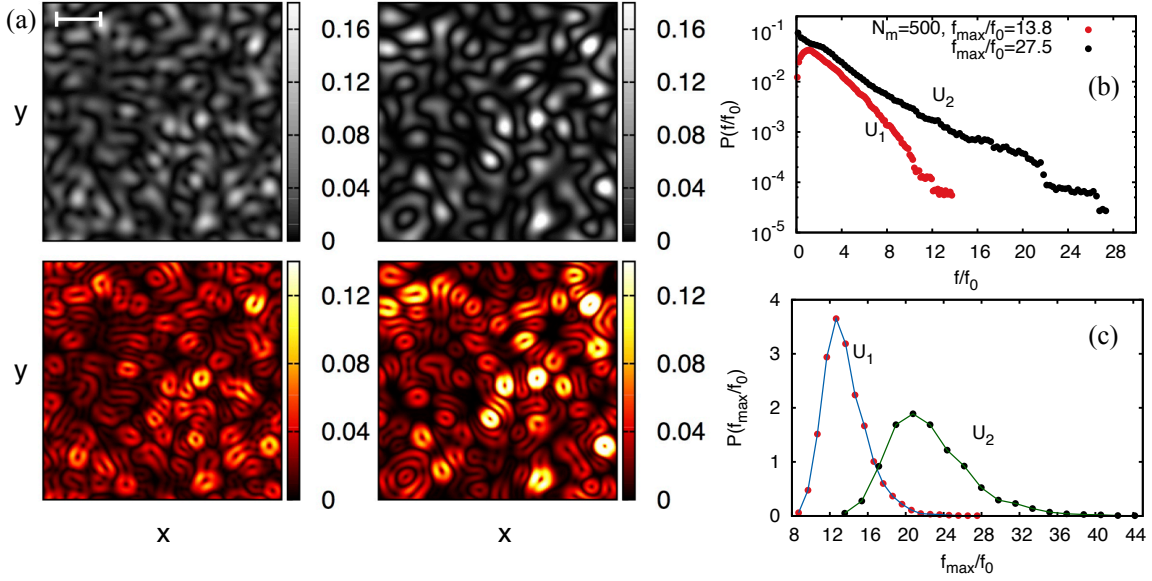


**Figure 1. Speckle patterns and force distributions.** Panel (a): in the top the two speckle patterns  $U_1$  (left) and  $U_2$  (right) used in the simulations ( $c = 0.165$ ). The scale for the intensity is  $\text{mW}\mu\text{m}^{-2}$ ; in the bottom we report the contour plot of the modulus of the force in pN. The white scale bar corresponds to  $30\mu\text{m}$ . Panel (b): distribution of the force of the sample used in the numerical simulations. Panel (c): distribution of the maximum of the force obtained averaging over  $N_s = 3000$  samples. The forces are expressed in unit of the self-propulsion of the swimmer  $f_0$ .

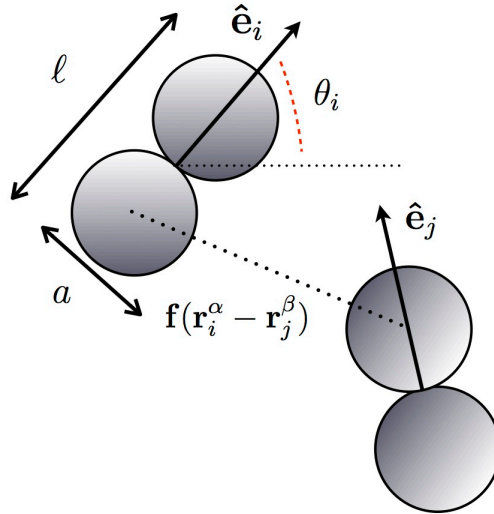


**Figure 2. Pictorial representation of the model.** Two swimmers, labelled by  $i$  and  $j$ , are modeled by a unit vector  $\mathbf{e}$  representing the swimming direction. Along the swimming direction are located two force-centers (beads) labelled by greek symbols  $\alpha = 1, 2$  (for the swimmer  $i$ ) and  $\beta = 1, 2$  for ( $j$ ). The interaction between two beads (of different swimmers) is short-ranged and repulsive.

At low Reynolds numbers regime [47, 48], the equations of motion are

$$\begin{aligned}\mathbf{v}_i &= \mathbf{M}_i \mathbf{F}_i \\ \boldsymbol{\omega}_i &= \mathbf{K}_i \mathbf{T}_i\end{aligned}\tag{7}$$

where  $\mathbf{v}_i$  is the center of the mass velocity and  $\boldsymbol{\omega}_i$  the angular velocity of the  $i$ -th swimmer.  $\mathbf{M}_i$  and  $\mathbf{K}_i$  are the translational and rotational mobility matrices

$$\begin{aligned}\mathbf{M}_i &= m_{\parallel} \hat{\mathbf{e}}_i \otimes \hat{\mathbf{e}}_i + m_{\perp} (\mathbb{1} - \hat{\mathbf{e}}_i \otimes \hat{\mathbf{e}}_i) \\ \mathbf{K}_i &= k_{\parallel} \hat{\mathbf{e}}_i \otimes \hat{\mathbf{e}}_i + k_{\perp} (\mathbb{1} - \hat{\mathbf{e}}_i \otimes \hat{\mathbf{e}}_i),\end{aligned}\tag{8}$$

the symbol  $\otimes$  is the dyadic product and  $\mathbb{1}$  the identity matrix. In Eq. (7),  $\mathbf{F}_i$  and  $\mathbf{T}_i$  are the total force and the total torque acting on the swimmer

$$\begin{aligned}\mathbf{F}_i &= f_0 \hat{\mathbf{e}}_i (1 - \sigma_i) + \sum_{j \neq i, \alpha, \beta} \mathbf{f}(\mathbf{r}_i^{\alpha} - \mathbf{r}_j^{\beta}) + \sum_{\alpha} \mathbf{f}_{ext}(\mathbf{r}_i^{\alpha}) \\ \mathbf{T}_i &= \mathbf{t}_r \sigma_i + \hat{\mathbf{e}}_i \times \left( \sum_{j \neq i, \beta \alpha} \delta^{\beta} \mathbf{f}(\mathbf{r}_i^{\alpha} - \mathbf{r}_j^{\beta}) + \sum_{\alpha} \delta^{\alpha} \mathbf{f}_{ext}(\mathbf{r}_i^{\alpha}) \right).\end{aligned}\tag{9}$$

The index  $j = 1, \dots, N$  runs over swimmers, the indices  $\alpha = 1, 2$  and  $\beta = 1, 2$  run over beads, and  $\sigma_i$  is a state variable, 0 for running swimmers and 1 for tumbling ones. The position of the beads of the  $i$ -th swimmers is

$$\mathbf{r}_i^{\alpha} = \mathbf{r}_i + \delta^{\alpha} \hat{\mathbf{e}}_i,\tag{10}$$

where

$$\delta^{\alpha} = (2\alpha - 3) \frac{\ell}{4}\tag{11}$$

giving rise to, i. e.,  $\delta^{1,2} = \pm \frac{\ell}{4}$ . The pair force  $\mathbf{f}(\mathbf{r})$  is the repulsive interaction among the swimmers (steric term)

$$\mathbf{f}(\mathbf{r}) = \frac{A \mathbf{r}}{r^{n+2}},\tag{12}$$

where the coefficient  $A$  is fixed by imposing that two swimmers facing head to head on the same line would be in equilibrium at the distance  $a$

$$A = f_0 a^{n+1}\tag{13}$$

where we choose  $n = 12$ . In Eq. (9) the external force  $\mathbf{f}_{ext}$  is given by expression (3) and  $f_0$  is the self-propulsion force. The two-state variables  $\sigma_i$  stochastically change with rate  $\lambda$  from the value 1 (tumbling state) to 0 (running state). In the tumbling state the  $i$ -th cell changes the free swimming direction due to a random torque  $\mathbf{t}_r$  acting for a finite tumbling-time  $\tau = \lambda^{-1}/10$  (this value of  $\tau$  is suitable for *E. coli* cells [27]), in the following we consider  $a = \ell/2$ . The system is enclosed in a square box of side  $L$  with periodic boundary conditions.

The equations of motion are numerically integrated for  $T = 100$ s by means of a second-order Runge-Kutta scheme with a time step  $\Delta t = 10^{-4}$ s. Choosing realistic parameters for *E. coli*, we have  $\ell = 3 \mu\text{m}$ ,  $m_{\parallel} = 60 \mu\text{m s}^{-1} \text{pN}^{-1}$ ,  $f_0 = 0.5 \text{ pN}$ , ( $v_0 = 30 \mu\text{m s}^{-1}$ ),  $\lambda^{-1} = 1 \text{ s}$  and  $\tau = 0.1 \text{ s}$ . To study the Brownian limit we change the time steps from

|                | $\ell$         | $a$              | $L$              | $\Delta t$        | $T$    | $\lambda^{-1}$ | $\tau$ | $v_0$                  | $f_0$ | $m_{\parallel}$                      | $m_{\perp}$                            | $k_{\perp}$              |
|----------------|----------------|------------------|------------------|-------------------|--------|----------------|--------|------------------------|-------|--------------------------------------|--|--------------------------|
| Internal Units | 1              | 1/2              | 50               | $10^{-3}$         | $10^3$ | 10             | 1      | 1                      | 1     | 1                                    | 0.87                                   | 4.8                      |
| Physical Units | $3\mu\text{m}$ | $1.5\mu\text{m}$ | $150\mu\text{m}$ | $10^{-4}\text{s}$ | 100s   | 1s             | 0.1s   | $30\mu\text{m s}^{-1}$ | 0.5pN | $60\mu\text{m s}^{-1}\text{pN}^{-1}$ | $52.2\mu\text{m s}^{-1}\text{pN}^{-1}$ | $31.3\mu\text{m s}^{-1}$ |

**Table 1. Internal and physical units.** Values (in internal and physical units) of the parameters used in the simulations.

$\Delta t = 10^{-4}\text{s}$  to  $\Delta t = 10^{-5}\text{s}$ . The mobility parameters are chosen as  $k_{\perp} = 31.3\mu\text{m s}^{-1}$ ,  $m_{\parallel} = 60\mu\text{m s}^{-1}\text{pN}^{-1}$  and  $m_{\perp} = 52.2\mu\text{m s}^{-1}\text{pN}^{-1}$  [41]. The relations between physical and internal units are reassumed in Tab. (1). Performing two dimensional simulations,  $k_{\parallel}$  does not play any role. We investigate non interacting and interacting swimmers at density,  $\bar{\rho} = N/L^2 = 0.018, 0.028\mu\text{m}^{-2}$  at fixed  $L = 150\mu\text{m}$ . The non-interacting case, i. e., a gas of run-and-tumble particles, is obtained switching off the steric potential. The Boltzmann limit is studied increasing tumbling rate  $\lambda^{-1} = 1.0, 0.25, 0.1, 0.025, 0.01\text{s}$  and free swimming velocity  $v = 30, 60, 94.9, 189.7, 300\mu\text{ms}^{-1}$ . The two fields  $U_1(\mathbf{r})$  and  $U_2(\mathbf{r})$  are generated by the same realization of  $N_m = 500$  wave vectors  $\mathbf{k}_l$  and phases  $\theta_l$ . The field is evaluated on a grid of  $10^5 \times 10^5$  points by means of parallel OpenMP algorithm.

### 3.2. Methods

For a given realization of the speckle fields, varying the intensity of the external forces through the parameter  $c$ , we investigate the ergodicity of the system looking at the behavior of dynamic observables, e. g., the correlation of the density fluctuations, and static observables, e. g., the density profiles and the probability distribution of the velocity.

The correlation of the density fluctuations is given by the intermediate scattering function. We compute both, the collective  $F_{coll}(\mathbf{q}, t)$  and the self  $F_{self}(\mathbf{q}, t)$  intermediate scattering function

$$F_{coll}(\mathbf{q}, t) = \frac{1}{N} \left\langle \sum_{l,m} \exp[-i\Delta\mathbf{r}_{lm}(t, t') \cdot \mathbf{q}] \right\rangle_{t'} \quad (14)$$

$$F_{self}(\mathbf{q}, t) = \frac{1}{N} \left\langle \sum_l \exp[-i\Delta\mathbf{r}_l(t, t') \cdot \mathbf{q}] \right\rangle_{t'}$$

with

$$\Delta\mathbf{r}_{lm}(t, t') \equiv \mathbf{r}_l(t + t') - \mathbf{r}_m(t') \quad (15)$$

The averaging is defined as follows

$$\langle \mathcal{O}(t) \rangle_t \equiv \frac{1}{T} \int_{t_0}^{T+t_0} dt \mathcal{O}(t) \quad (16)$$

and the initial time  $t_0$  is chosen such that  $t_0 > \lambda^{-1}$ . In our simulations we take  $t_0 = 5\text{s}$ .

Varying the intensity of the external field, a finite number of swimmers spend more and more time in the minima of the random-energy landscape. Looking at the long-time

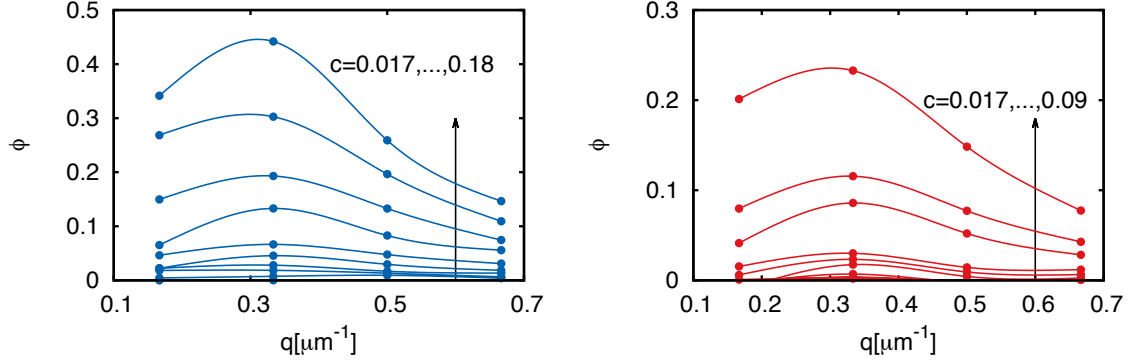


**Figure 3. The ergodicity parameter at different wavenumbers.** Ergodicity parameter  $\phi$  as a function of  $q$  for the pattern  $U_1$  (left panel) and  $U_2$  (right panel) at different values of  $c$ . Continuous lines are obtained by spline interpolation.

behavior of  $F_{coll}(\mathbf{q}, t)$  we define the ergodicity parameter as follows [49]

$$\phi(c, q) \equiv \lim_{t \rightarrow \infty} F_{coll}(\mathbf{q}, t). \quad (17)$$

The ergodicity parameter gives a measure of the fraction of swimmers localized on the spatial scale  $R_b \sim 1/q$ . In Fig. (3) we show the dependency of  $\phi$  on  $q$  for  $U_1$  (left panel) and  $U_2$  (right panel). The peak developed by  $\phi$  at  $q \sim 0.3 \mu\text{m}^{-1}$  signals the spatial scale of the regions of maximum speckle intensity.

To study the static properties of the model we start from the density profile defined as

$$\rho(\mathbf{r}) = \frac{1}{\mathcal{V}} \left\langle \sum_i \delta(\mathbf{r} - \mathbf{r}_i(t)) \right\rangle_t, \quad (18)$$

the normalization factor  $\mathcal{V}$  is fixed by the condition

$$\int d\mathbf{r} \rho(\mathbf{r}) = 1. \quad (19)$$

The entropy of the distribution  $\rho(\mathbf{r})$  reads

$$s[\rho] = - \int d\mathbf{r} \rho(\mathbf{r}) \log \rho(\mathbf{r}) \quad (20)$$

which, for  $c \rightarrow 0$ , reduces to

$$\lim_{c \rightarrow 0} s[\rho] = \log V \quad (21)$$

with  $V = L^2$ .

Steady states for run-and-tumble particles are in general non-Boltzmann. The Boltzmann case can be obtained in the limit  $\lambda, v_0 \rightarrow \infty$  with constant  $v_0^2/2\lambda$ . In the Boltzmann limit, the density profile in presence of the speckle field  $U_i(\mathbf{r})$ , ignoring the excluded volume interaction, is

$$\rho_B(\mathbf{r}) = \frac{e^{-\frac{U_i(\mathbf{r})}{k_B T_{eff}}}}{Z} \quad (22)$$



with  $i = 1, 2$ . The normalization is

$$Z = \int d\mathbf{r} e^{-\frac{U_i(\mathbf{r})}{k_B T_{eff}}} \quad (23)$$

The entropy of the distribution is

$$s[\rho_B] = - \int d\mathbf{r} \rho_B(\mathbf{r}) \log \rho_B(\mathbf{r}) \quad (24)$$

and in the limit  $c \rightarrow 0$  one has

$$\lim_{c \rightarrow 0} s[\rho_B] = \log V = \lim_{c \rightarrow 0} s[\rho]. \quad (25)$$

We compare the equilibrium properties of the isodiffusive simulations with the Boltzmann limit expressed by Eq. (22) with  $k_B T_{eff} = D/\mu$ .

Another static observable which gives information about the density inhomogeneities, is the probability distribution of velocity for cells in the running state ( $\sigma_i = 0$ )

$$P(v) = \frac{1}{\mathcal{N}} \left\langle \sum_i \delta(v - v_i(t) | \sigma_i = 0) \right\rangle_t \quad (26)$$

with  $v = |\mathbf{v}|$ ,  $v_i(t) = |\mathbf{v}_i(t)|$  and  $\mathcal{N}$  fixed by the condition

$$\int dv P(v) = 1. \quad (27)$$

From the behavior of  $P(v)$  at small  $v$  we obtain information about the fraction of particles locked by the field.

Finally, to study the transport properties of the system, we look at the mean-square displacement

$$msd = \frac{1}{N} \left\langle \sum_i [\mathbf{r}_i(t + t') - \mathbf{r}_i(t')]^2 \right\rangle_{t'}. \quad (28)$$

## 4. Results

The speckles concentrates  $\rho(\mathbf{r})$  in the minima of the random energy landscape. In Fig. (4) we show the density fields at different values of the control parameter  $c$  in the cases of speckle fields  $U_1(\mathbf{r})$  (left panel) and  $U_2(\mathbf{r})$  (right panel). For the data shown in figure, the average bacterial density is  $\bar{\rho} = 0.018 \mu\text{m}^{-2}$ . In the homogeneous phase ( $c = 0.017$  in Fig. (4)), the system is ergodic and the density is uniform in space. Increasing the intensity of the external field, density profiles become inhomogeneous and the bright spots in Fig. (4) indicate that the system spends more and more time in the minima of the random energy landscape.

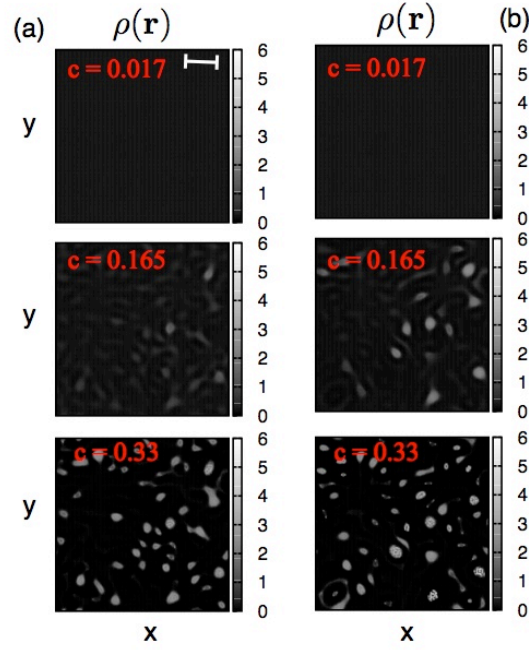


**Figure 4. Density profiles at different speckle intensities.** Comparison between density profiles for  $U_1(\mathbf{r})$  (panel (a)) and  $U_2(\mathbf{r})$  (panel (b)) for three values of the control parameter  $c$ . The density field  $\rho(\mathbf{r})$  is modulated by the random energy landscape, increasing the intensity of the external field the system spends more and more time in the minima of the external potential breaking the ergodicity at high  $c$ . The white scale bar corresponds to  $30\mu\text{m}$ .

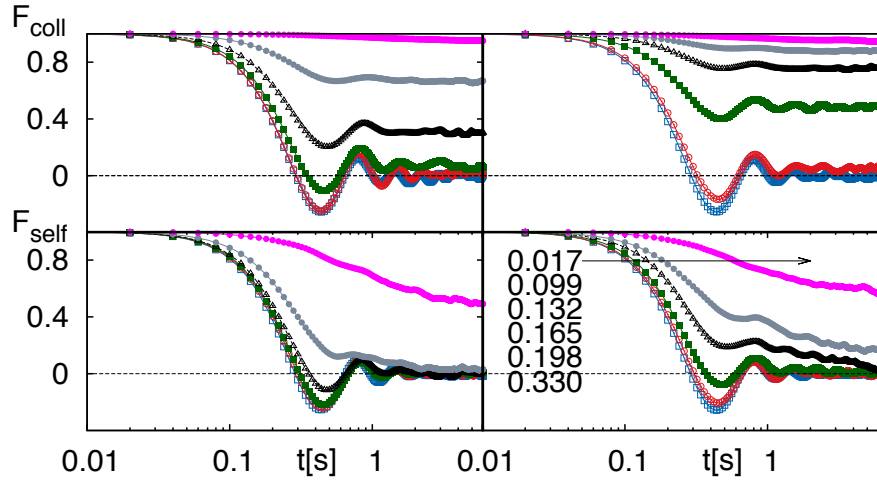


**Figure 5. Intermediate Scattering Functions.** Collective and self part of the Intermediate Scattering function for  $U_1(\mathbf{r})$  (left panels) and  $U_2(\mathbf{r})$  (right panels) for  $q = 0.3\mu\text{m}^{-1}$  at different values of  $c$  from  $c = 0.017$  (blue) to  $0.330$  (magenta).

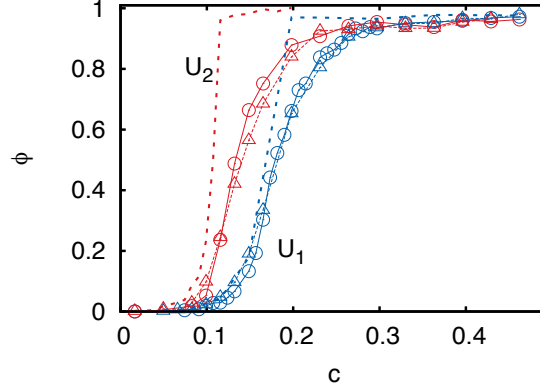


**Figure 6. Ergodicity parameter as a function of the speckle intensity.** The dashed lines are the non-interacting (ideal gas of run-and-tumble bacteria) simulations, the circles represent simulations performed at density  $\bar{\rho} = 0.018 \mu\text{m}^{-2}$  (triangle  $\bar{\rho} = 0.028 \mu\text{m}^{-2}$ ).

#### 4.1. Threshold estimation

In Fig. (5) we report the collective (top of the figure) and self (bottom) part of the intermediate scattering function as a function of time at different intensities of the speckle in the case of  $N = 400$  swimmers ( $\bar{\rho} = 0.018 \mu\text{m}^{-2}$ ) and  $q = 0.3 \mu\text{m}^{-1}$ . Starting from  $c \sim 0.132$  for the potential  $U_1$  ( $\sim 0.099$  for  $U_2$ ), the collective part of the intermediate scattering function develops a plateau that continuously increases from 0. Looking at the self correlation, in the range of  $c$  where one has  $\phi \neq 0$ ,  $F_{self}(q, t)$  decays to zero, indicating that the single bacterium escapes from the energy barriers. At high enough values of  $c$ ,  $F_{self}(q, t)$  too does not decay to zero and a finite fraction of bacteria are trapped. The threshold value  $c_\phi^*$  has been defined looking at the maximum of  $d\phi/dc$ . The behavior of  $\phi$  as a function of  $c$  is shown in Fig. (6) for  $\bar{\rho} = 0.018, 0.028 \mu\text{m}^{-2}$  and for non-interacting swimmers. Looking at the interacting case, one has that the density does not play a crucial role on the trapping. Comparing the interacting bacteria with the non-interacting ones, we observe that the excluded volume smooths the transition. We obtain  $c_\phi^* = 0.165$  for  $U_1$  and  $c_\phi^* = 0.116$  for  $U_2$ .

Looking at the entropy defined by Eq. (20), we can give another estimation of the threshold value  $c^*$ . In Fig. (7), we show the entropy as a function of  $c$  for the speckle patterns  $U_1$  and  $U_2$  (top of the figure). The derivative of the entropy with respect to  $c$  is shown in the bottom of Fig. (7). The crossover value, defined as the minimum of  $ds/dc$ , is  $c_s^* = 0.215$  for  $U_1$  and  $0.165$  for  $U_2$ .

A qualitative estimation of crossover value  $c^*$  can be also obtained from the probability distribution function of velocity defined by Eq. (26). Since  $P(v)$  is computed by considering only particles in running state, the peak at low velocities is due to the fraction of trapped particles and the height is proportional to the number of particles in the minima of the potential. In Fig. (8) we report  $P(v)$  for  $U_1$  (left panel) and  $U_2$  (right panel). Increasing the intensity of the external field, the probability distribution of

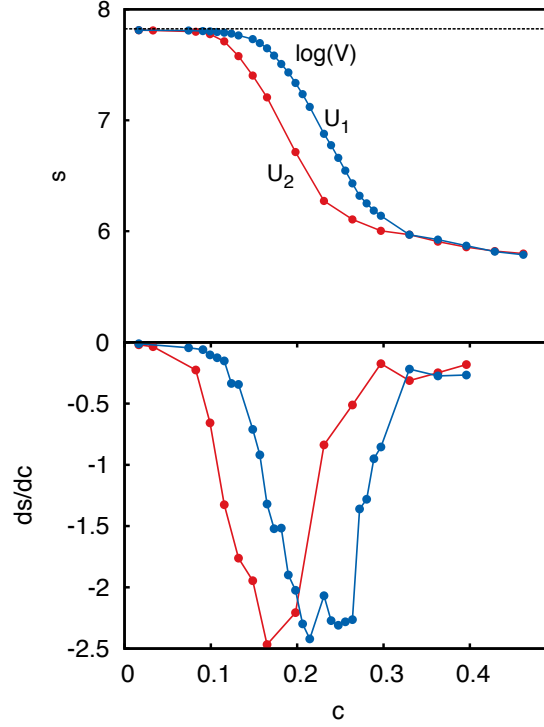


**Figure 7. Entropy as a function of the speckle intensity.** Top panel: the entropy computed using Eq. (20) varying the intensity of the speckle patterns. Bottom panel: derivative of the entropy with respect the control parameter  $c$ .

|       | $c_s^*$ | $c_\phi^*$ | $c_v^*$ | $c_{max}$ |
|-------|---------|------------|---------|-----------|
| $U_1$ | 0.215   | 0.165      | 0.198   | 0.190     |
| $U_2$ | 0.165   | 0.116      | 0.165   | 0.135     |

**Table 2.** Threshold values for the intensity of the speckles  $U_1$  and  $U_2$ . Estimation through the derivative of the entropy ( $c_s^*$ ), the derivative of the ergodicity parameter ( $c_\phi^*$ ), looking at the probability distribution of the velocity ( $c_v^*$ ) and by the maximum force of the speckle pattern.

velocity shows two peaks due to the competition between self-propulsion and trapping. The peak at high velocity is due to the self-propulsion and it is less pronounced for the pattern  $U_1$ .

We can heuristically define  $c_v^*$  as the value of  $c$  for which  $P(v)$  becomes flat at low  $v$ . We have  $c_v^* \sim 0.198$  for  $U_1$  and  $\sim 0.165$  for  $U_2$ . The threshold values are summarized in Tab. (2). The last column reports  $c_{max}$ , defined as the value of  $c$  where the maximum force of the speckle  $f_{max}$  is equal to the self-propulsion of the swimmer. As one can see, all the values  $c^*$  are of the same order of magnitude of  $c_{max}$ . Comparing the crossover values of  $c$  for  $U_1$  and  $U_2$  we can conclude that the pattern generated by  $U_2$  spends less energy than  $U_1$  to trap. This is due to the tails in the distribution of the forces shown in Fig. (1) and it is in agreement with the statistical properties of the distribution of the maximum force reported in Sec. (2).

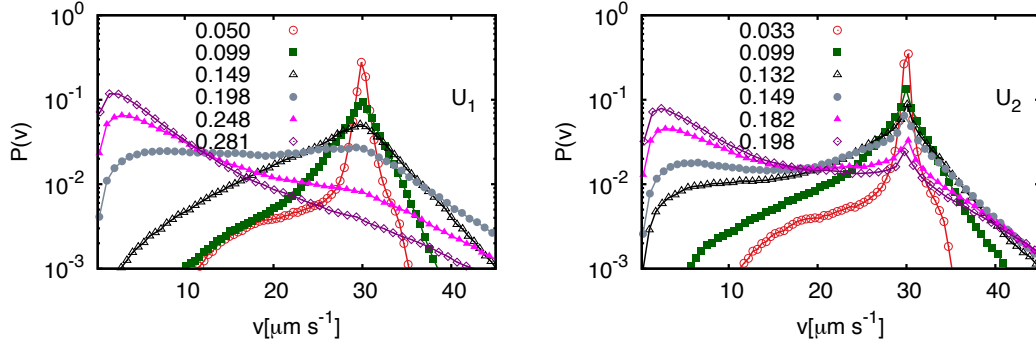


**Figure 8. Probability distribution of velocity.** Probability distribution of velocity for particles in the run-state in the presence of potentials  $U_1(\mathbf{r})$  ( $U_2(\mathbf{r})$ , right panel) at different  $c$ .

#### 4.2. Comparison with the Boltzmann limit

In this section we investigate the relation between run-and-tumble dynamics on long time and Boltzmann equilibrium. Run-and-tumble dynamics is diffusive on long time, on the other hand at the equilibrium the probability distribution becomes Boltzmann only in limit cases [37, 31]. The steric interaction changes the value of the diffusivity from  $D$  to  $D_{int}$  with  $D_{int} \leq D$  [36] that can be obtained by the mean-square displacement

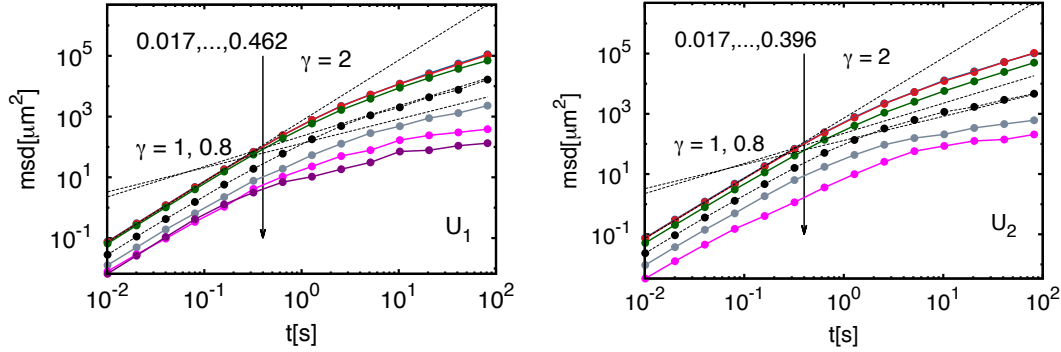


**Figure 9. Subdiffusive regime at high intensities.** Mean-square displacement for  $U_1(\mathbf{r})$  ( $U_2(\mathbf{r})$ , right panel) at different  $c = 0.017, 0.083, 0.165, 0.248, 0.330, 0.396, 0.462$  for  $U_1$  and  $c = 0.017, 0.083, 0.165, 0.248, 0.330, 0.396$  for  $U_2$ . The dashed lines show the crossover between ballistic and diffusive regime. At high  $c$  the diffusive regime becomes subdiffusive.

given by Eq. (28). In the long-time limit one has:

$$msd \sim D_{int} t^\gamma. \quad (29)$$

In Fig. (9) we show the mean-square displacement at different  $c$  for  $U_1$  and  $U_2$ . We observe normal diffusion ( $\gamma = 1$ ) at small speckle intensity, and subdiffusion ( $\gamma < 1$ ) at higher intensities. It is known in literature that Brownian particles embedded into random energy landscape show a subdiffusive regime [9, 11, 19, 20, 21, 22], and, in

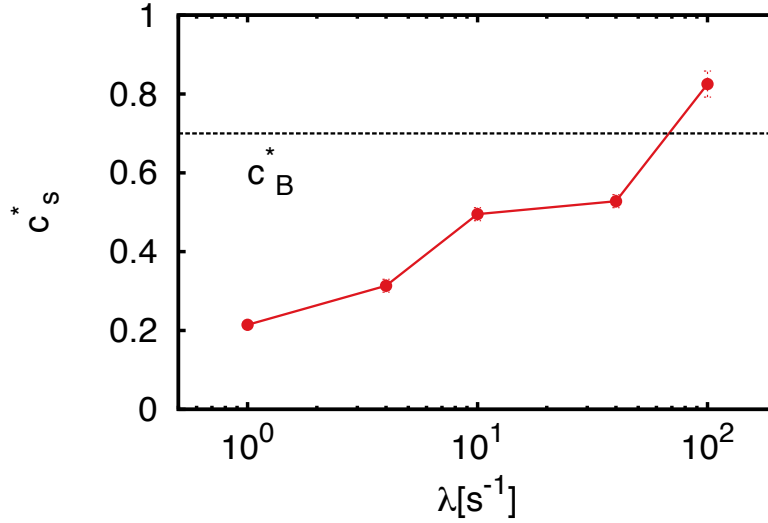


**Figure 10. Threshold values as a function of the tumbling rate.** The threshold values are computed looking at the derivative of the entropy with respect to the control parameter  $c$ . Increasing the tumbling rate (keeping the diffusion coefficient fixed) one has to increase the intensity of the speckles to trap the particles. The dashed line is the Boltzmann limit ( $\lambda \rightarrow \infty$ ) for non-interacting particles.

our model, the subdiffusion emerges when the maximum force exerted by the speckles overcomes the self-propulsion.

We study the Brownian limit of the run-and-tumble dynamics increasing the tumbling rate  $\lambda$  and the velocity  $v_0$ . We perform numerical simulations for  $\lambda^{-1} = 1.0, 0.25, 0.1, 0.025, 0.01$  s and the self propulsion velocity is changed according to  $v = \sqrt{2\lambda D}$ . Embedding the system into the speckle pattern  $U_1$  and varying  $c$ , we look at the entropy to compute the threshold value  $c_s^*(\lambda)$ , the results being shown in Fig. (10). As we can see, increasing the tumbling rate we have to increase the intensity of the speckle in order to trap the particles. In Fig. (10) we also report the crossover value  $c_B^*$  obtained considering the Boltzmann limit of dilute (ideal gas) run-and-tumble particles. It is worth noting that for the higher  $\lambda$  value one has  $c^*(\lambda = 100) > c_B^*$ , may be due to the excluded volume effects, not included to estimate  $c_B$ .

## 5. Conclusions

We have numerically investigated steric-interacting run-and-tumble particles embedded in random energy landscapes generated by speckle fields. The main result is the appearance of a crossover that separates the non-trapped to the trapped regime upon increasing speckle intensity. The crossover value for the external field  $c^*$  can be estimated from the behavior of dynamical observables, as the collective density fluctuations  $F_{coll}(q, t)$  or static observables, as the density profiles  $\rho(\mathbf{r})$ , the entropy of the density distribution  $s[\rho]$  and the probability distribution of the velocity  $P(v)$ . The obtained

threshold  $c^*$  values are of the same order of magnitude of  $c_{max}$ , i. e., the value of  $c$  for which the maximum force exerted on the system by the speckles equals the self-propulsion force of the bacterium. For large values of the intensity, the dynamics of the model becomes subdiffusive. The study is performed by means of two types of patterns namely,  $U_1$  —the standard speckle pattern— and  $U_2$ , i.e., the speckle due to only the real part of the electric field. The patterns are generated using the same configuration of wave-vectors and phases and the fields have the same energy. From our analysis follows that pattern  $U_2$  traps more efficiently than  $U_1$ .

We have compared the results respect to those obtained in the Boltzmann regime. Increasing the tumbling rate  $\lambda$  and the velocity  $v$  at fixed diffusivity  $D = v^2/2\lambda$ , we have studied the Brownian limit of the model, comparing the static properties obtained with the Boltzmann statistics at the effective temperature  $T_{eff}$ . In absence of steric interaction, the Boltzmann measure is concentrated in the minima of the potential. Entropy decreases and the derivative  $ds/dc$  shows a minimum at  $c_B^* > c^*$ . As a consequence, in order to trap Brownian particles (driven by the dynamics to the Boltzmann equilibrium) we have to increase the intensity of the speckles with respect to the case of active particles.

## Acknowledgments

We acknowledge support from MIUR-FIRB project RBFR08WDBE. The research leading to these results has received funding from the European Research Council under the European Union's Seventh Framework Programme (FP7/2007-2013) / ERC grant agreement n° 307940. MP thanks to S. Roldán-Vargas for many stimulating discussions.

## References

- [1] A. Ashkin, Phys. Rev. Lett. **24**, 156 (1970).
- [2] A. Ashkin, Proc. Natl. Acad. Sci. **94**, 4853 (1997).
- [3] D. M. Stamper-Kurn, M. R. Andrews, A. P. Chikkatur, S. Inouye, H.-J. Miesner, J. Stenger, and W. Ketterle, Phys. Rev. Lett. **80**, 2027 (1998).
- [4] A. Ashkin, and J. M. Dziedzic, Science **20** 1517 (1987).
- [5] D. G. Grier, Nature **424**, 810 (2003).
- [6] M. J. Padgett, and R. Di Leonardo, Lab Chip **11**, 1196 (2011).
- [7] V. G. Shvedov, A. V. Rode, Y. V. Izdebskaya, D. Leykam, A. S. Desyatnikov, W. Krolikowski, and Y. S. Kivshar, J. Opt. **12**, 124003 (2010).
- [8] I. M. Sokolov, Soft Matter **8**, 9043 (2012).
- [9] J.-P. Bouchaud and A. Georges, Phys. Rep. **195**, 127 (1990).
- [10] D. S. Dean, I. T. Drummond, and R. R. Horgan, J. Stat. Mech. (2007) P07013.
- [11] R. Zwanzig, Proc. Natl. Acad. Sci. **85**, 2029 (1988).
- [12] S. Havlin and D. Ben-Avraham, Adv. Phys. **36**, 695 (1987).
- [13] M. B. Isichenko, Rev. Mod. Phys. **64**, 961 (1992).
- [14] A. Heur, J. Phys.: Condens. Matter **20** 373101 (2008).
- [15] R. L. Jack and P. Sollich, J. Stat. Mech. (2009) P11011.
- [16] J. Bernasconi, H. U. Beyeler, S. Strassler, and S. Alexander, Phys. Rev. Lett. **42**, 819 (1979).
- [17] E. Barkai, Y. Garini, and R. Metzler, Phys. Today **65** 29 (2012).

- [18] J. W. Haus, K. W. Kehr, and J. W. Lyklema, Phys. Rev. B **25**, 2905 (1982).
- [19] D. S. Novikov, E. Fieremans, J. H. Jensen, and J. A. Helpert, Nature Phys. **7**, 508 (2011).
- [20] R. D. L. Hanes, C. Dalle-Ferrier, M. Schmiedeberg, M. C. Jenkins, and S. U. Egelhaaf, Soft Matter **8**, 2714 (2012).
- [21] R. D. L. Hanes and S. U. Egelhaaf, J. Phys.: Condens. Matter **24**, 464116 (2012).
- [22] F. Evers, C. Zunke, R. D. L. Hanes, J. Bewerunge, I. Ladadwa, A. Heuer, and S. U. Egelhaaf, Phys. Rev. E **88**, 022125 (2013).
- [23] G. Volpe, G. Volpe, and S. Gigan, Scient. Rep. **4**, 3936 (2014).
- [24] O. Chepizhko, and F. Peruani, Phys. Rev. Lett. **111**, 160604 (2013).
- [25] C. Reichhardt, and C.J. O. Reichhardt, <http://arxiv.org/abs/1402.3260> (2014).
- [26] M. J. Schnitzer, Phys. Rev. E **48**, 2553 (1993).
- [27] H. C. Berg, *E. coli In Motion* (Springer, New York, 2004).
- [28] H. C. Berg, D. A. Brown, Nature (London) **239**, 500 (1972).
- [29] N. Koumakis, A. Lepore, C. Maggi, R. Di Leonardo, Nature Communications, **4**, 2588 (2013).
- [30] R. Di Leonardo, L. Angelani, D. Dell'Arciprete, G. Ruocco, V. Iebba, S. Schippa, M. P. Conte, F. Mecarini, F. De Angelis, and E. Di Fabrizio, Proc. Natl. Acad. Sci. **107**, 9541 (2010).
- [31] M. E. Cates, Rep. Prog. Phys. **75**, 042601, (2012).
- [32] C. Reichhardt, and C.J. O. Reichhardt, Phys. Rev. E **88**, 042306 (2013).
- [33] M. B. Wan, C.J. O. Reichhardt, Z. Nussinov, and C. Reichhardt, Phys. Rev. Lett. **101**, 018102 (2008).
- [34] L. Angelani, Europhys. Lett. **102**, 20004 (2013).
- [35] K. Martens, L. Angelani, R. Di Leonardo and L. Bocquet, Eur. Phys. J. E **35**, 84 (2012).
- [36] M. Paoluzzi, R. Di Leonardo, and L. Angelani, J. Phys.: Condens. Matter **25** 415102 (2013).
- [37] J. Tailleur, and M. E. Cates, Europhys. Lett. **86**, 60002 (2009).
- [38] L. Angelani, A. Costanzo and R. Di Leonardo, EPL **96**, 68002 (2011).
- [39] L. Angelani, R. Di Leonardo, and M. Paoluzzi, *in preparation*.
- [40] J. Tailleur, and M. E. Cates, Phys. Rev. Lett. **100**, 218103 (2008).
- [41] L. Angelani, R. Di Leonardo and G. Ruocco, Phys. Rev. Lett. **102**, 048104 (2009).
- [42] L. Angelani and R. Di Leonardo, New Journal of Physics **12**, 113017 (2010).
- [43] L. Angelani and R. Di Leonardo, Comp. Phys. Commun. **182**, 1970 (2011).
- [44] C. Maggi, A. Lepore, J. Solari, A. Rizzo, and R. Di Leonardo, Soft. Matt. **9**, 10885 (2013).
- [45] J. Goodman, Speckle Phenomena in Optics: Theory and Applications, Roberts & Company Publishers, (2010).
- [46] Y. Harada, and T. Asakura, Opt. Commun. **124**, 529 (1996).
- [47] E. M. Purcell, Am. J. Phys. **45**, 3 (1977).
- [48] S. Kim and S. Karrila, *Microhydrodynamics* (Dover, New York, 2005).
- [49] W. Götze, in: J.P. Hansen, D. Levesque, J. Zinn-Justin (Eds.), Liquids, Freezing and Glass Transition, North-Holland, Amsterdam, p. 287 (1991).